Postharvest Biology and Technology, Volume 213, July 2024, Article number 112977
DOI: 10.1016/j.postharvbio.2024.112977

Investigation of the horizontal collision damage behavior of fruit during transporting based on a new instrumented impactor

Minggang Wang[a], Mingwei Shi[a], Tobi Fadiji[b,*], Zhiguo Li[a,*] Guoxiong Song[c]

[a] *College of Mechanical and Electronic Engineering, Northwest A&F University, Yangling, 712100, China*

[b] *Plant Science Laboratory, Cranfield University, Cranfield MK43 0AL, United Kingdom*

[c] *Agricultural Machinery Technology Promotion Service Center of Yan'an, Yan'an, 716000, China*

**Correspondence Email: lizhiguo0821@163.com (*Z. Li*), tobi.fadiji@cranfield.ac.uk (Tobi)*

Abstract: Horizontal collisions between fruit and rigid walls are a common occurrence in postharvest packaging and transportation. To address this issue, a novel high-precision instrumented impactor was developed, comprising a high-speed imaging system, an ejection device, and a force sensor. Results showed that the impactor was able to effectively simulate the horizontal collision process between various small spherical fruits (such as cherry tomatoes, plums, sweet cherries, and winter jujubes) and packaging materials at three velocities: slow, medium, and high. Output parameters included the impact force and impact time of the fruit acting on each packaging material, as well as the displacement, displacement rate, impact energy, rebound energy, and absorption energy of the fruit. During the horizontal collision simulation, it was observed that the winter jujube exhibited the largest impact force and the shortest impact time among the four types of fruit tested. Conversely, the sweet cherry demonstrated the lowest proportion of damage area when colliding with the EPE board compared to the rigid board and foam board. This study presents a powerful tool for investigating the horizontal collision behaviour between fruit and rigid plates.

Keywords: Texture; Postharvest handling; Impact behavior; Simulation; Biomechanics

Published by Elsevier. This is the Author Accepted Manuscript issued with: Creative Commons Attribution License (CC:BY 4.0).
The final published version (version of record) is available online at DOI:10.1016/j.postharvbio.2024.112977. Please refer to any applicable publisher terms of use.

Nomenclature

A_d	percentage of damaged area	S_0	total cross-sectional area of the fruit's pedicel, mm^2
A_{m1}	mass loss rate after 1 d	t_I	impact time for different collision types, ms
A_{m2}	mass loss rate after 2 d	t_C	compression time, ms
B_d	susceptibility to bruising in fruit, mm^2/J	μ_f	friction coefficient between fruit and ejection port
E_0	energy absorption, J	v_b	speed of the steel ball, m/s
E_L	energy loss from inelastic collision, J	v_f	theoretical horizontal launch velocity of the fruit, m/s
E_1	impact energy of the fruit, J	v_0	average initial velocity of the fruit, m/s
E_2	rebound energy of the fruit, J	v_1	average rebound velocity of the fruit, m/s
F	impact force, N	x_0	displacement of the fruit in time Δt_0, m
F_{max}	maximum impact force, N	x_1	displacement of the fruit in time Δt_1, m
g	gravitational acceleration, m/s^2	Δt_0	time taken for fruit motion in 10 frames after the start frame, s
m_b	quality of steel balls, kg	Δt_1	time taken for fruit to rebound in motion for 5 frames after leaving the rigid plate, s
m_f	mass of the fruit before impact, kg	ϵ	relative error
m_s	quality of rigid pads, kg		
m_{d1}	mass loss of the fruit on the first day, kg		
m_{d2}	mass loss of the fruit on the second day, kg		
S_f	the distance of the fruit slides before leaving the ejection port, m		
S_d	area of the region where damage occurs and turns brown, mm^2		

22

1 Introduction

Mechanical damage to fruit mainly includes four types: impact damage, compression damage, abrasion damage, and puncture damage (Li and Thomas., 2014; Paulsen et al.,2021). Among them, impact damage is the most severe type in postharvest fruit processing (Van Zeebroeck et al., 2007; Ahmadi et al.,2012; Zhou et al.,2016). During transportation, sudden acceleration or braking can result in horizontal collisions among fresh fruit, causing the rupture or separation of internal cells and leading to impact damage (Ortiz and Torregrosa., 2014; Wang et al., 2020; Preuk et al., 2019). The macroscopic signs of impact damage typically manifest as surface bruises or cracks (Polat et al., 2007). These injuries create favorable conditions for rapid microbial growth and reproduction within the damaged area, accelerating fruit quality deterioration and hastening decay. Ultimately, this renders the fruit commercially valueless (Tian, SP., et al.,2001; Cevher and Oztekin.,2022; Chen et al.,2023）. Consequently, studying the horizontal collision damage behavior of fruit during transporting holds significant scientific value.

Currently, research on impact loads often employs methods such as free-fall and pendulum tests. These methods involve either attaching a fruit to the pendulum or using a pendulum equipped with a specific-shaped impactor to strike stationary fruit. Hussein et al. (2019) investigated the sensitivity of vertical impact damage in three different pomegranate varieties from various heights using the free-fall method. Sun et al. (2021) conducted free-fall tests of tomatoes from different heights onto cylindrical cardboard surfaces to study the sensitivity of vertical impact damage in tomatoes, considering variables such as fruit size, falling height, and detection time points. Xu et al. (2015) employed blueberry impact recording device to record vertical impact damage incurred by blueberries of four different varieties dropped from varying heights. Measurement data revealed that the degree

of damage was related to falling height (impact velocity) and cushioning material. Oztekin and Gungor. (2020) simulated vertical impacts of peaches against the surfaces of commercial packaging devices using free-fall tests. The results indicated that polyurethane foam material was more suitable as a fruit collision cushioning material than foam rubber. Van Zeebroeck et al. (2007) conducted tomato impact tests using a pendulum test apparatus. The test specimens were affixed to anvils using elastic bands during the experiment, leading to the development of linear and nonlinear regression damage prediction models for the "tradro" variety. Wang et al. (2018) conducted impact tests on lychee fruit of two varieties using a pendulum testing apparatus. The authors found that both the frequency and velocity of impacts affect the degree of mechanical damage to the fruit. Stropek. and Golacki. (2019) introduced a novel method for securing fruit to a pendulum, specifically fastening pears with screws onto a pendulum composed of fishing lines. The research revealed that the progression speed of bruising depended on the fruit's hardness. Fu et al. (2020) designed a specialzed pendulum-type device to quantitatively assess the severity of fruit bruising caused by apple-to-apple impacts at different zones on the apple surface.

To sum up, while the current literature has advanced significantly in simulating fruit impact and damage processes through conventional free-fall and pendulum methods, there remains a gap for an instrumented horizontal impactor capable of directly assessing horizontal impact damage on small spherical fruit while in a free state and with a specific initial velocity. To investigate the horizontal impact damage behavior during small spherical fruit transportation more realistically, this paper leverages design insights from previous pendulum test devices and enhances them in the following four aspects: (1) The use of this instrumented horizontal impactor eliminates the need for fixing the fruit during the simulated impact process, aligning with scenarios where fruit impacts packaging

materials in a free-moving state on transportation and commodity packaging lines. (2) The instrumented horizontal impactor incorporates sensors on a rigid plate and is equipped with a camera system to monitor the complete movement of the fruit in real time, enabling the distinct observation of the entire inelastic impact process of the fruit and the differentiation of damage areas. (3) During the impact test using this instrumented horizontal impactor, the fruit's mass and impact speed are direct output parameters, and the impact energy can be calculated more accurately. (4) Some pendulum test apparatuses theoretically necessitate constant adjustment of the pendulum string length to ensure that the pendulum strikes the fruit horizontally at its lowest point, leading to a relatively cumbersome operation. In contrast, this instrumented horizontal impactor enables the test fruit to gain initial speed through the launching device and is relatively simple to operate. Therefore, the aim of this study is to develop a new instrumented horizontal impactor for investigating the horizontal collision damage behavior between small spherical fruit and packaging materials during transportation.

2 Materials and methods

2.1 Design concept for the instrumented horizontal impactor

The problem of impact damage to fruit is the most severe challenge encountered during fruit harvesting, packaging, and transportation, particularly in transportation scenarios characterized by horizontal collisions between fruit and the packaging container walls, which typically result from rapid acceleration or braking (Van Zeebroeck et al., 2008; Dintwa et al., 2008; Zhang et al., 2018). From an engineering simulation perspective, to investigate the problem of horizontal impact on fruit, it is essential to simulate the impact and damage process in the horizontal direction experienced by these fruits. Based on a dynamics-related standpoint, accurately capturing the force dynamics during

the horizontal impact and damage process of fruit necessitates imparting appropriate initial velocities to these fruits, causing them to collide with rigid surfaces. Simultaneously, recording the impact force and impact time on the rigid collision surface throughout the collision process is crucial. From a kinematics perspective, to capture the motion state of fruit during horizontal impact and damage processes, a high-speed camera system was employed to record the entire trajectory and movement of the fruit throughout the collision process. Therefore, the design concept of this study, as illustrated in Fig. 1, encompassed several key steps. Firstly, fresh fruit were securely affixed to a launching device containing a spring within the launching tube, generating an impact force when the launching rod was compressed and released. To provide different horizontal initial velocities for the ejection device, the ejection rod was designed with three slots at various positions: left, middle, and right. By positioning the grooves of the ejection handle within these slots, different levels of spring compression were achieved, yielding three speed levels for the fruit: high speed, medium speed, and slow speed, respectively. This configuration ensured that the fruit remained in a free state during movement, replicating real-world conditions. Secondly, a power supply unit delivered energy to the entire instrumented horizontal impactor. Finally, a force data acquisition system recorded the impact force on the rigid surface in real time during the collision process, while a high-speed camera system captured the entire motion state of the fruit in real time.

2.2 The development of the instrumented horizontal impactor

2.2.1 The structural design of the instrumented horizontal impactor

Based on the above ideas, this study independently developed a novel instrumented horizontal impactor for fruit (Fig. 2). This new instrumented horizontal impactor included one power supply system, one launching device, one force data acquisition system, one high-speed camera system, and one framework. The high-speed camera system was installed on both sides of the top plate of the

framework, and the launching device and force data acquisition device were mounted on the middle plate. The switch-mode power supply, data acquisition card, and signal amplifier were installed in the lower control box of the framework. The force sensor data cable was connected through the middle plate's cable hole to the signal amplifier in the control box. The Universal Serial Bus data cable connected the data acquisition card to the computer through the rear cable hole of the framework, forming the entire instrumented horizontal impactor.

The integrated framework design facilitated assembly, device placement, and testing and prevented the fruit from falling off the instrumented horizontal impactor and colliding with the ground or other objects after impact testing. The power supply system comprised a switch-mode power supply and a transformer. The launching device mainly consisted of one ejection port chuck (PLA), one rigid pad (PLA), one support base, and one launcher. The force data acquisition system included one rigid surface (PLA), one support plates, one movable platform, one ruler, one flat membrane box-type pressure sensor (JHBM-H1, Bengbu Jinnuo Sensor Co., Ltd., China), one control box, one signal amplifier (BSQ-2, Bengbu Jinnuo Sensor Co., Ltd., China), one data acquisition card (USB-3100 N, Altai Technology Development Co., Ltd., China) and a computer. The monitoring and acquisition of the transmitter's electrical signal during the impact process were performed using the accompanying measurement and control software. According to impact theory, when two objects collide, if the hardness of object B is greater than that of object A and object B undergoes minimal deformation, it can be considered relatively rigid. PLA is known for its high stiffness, high modulus and brittleness (Shi et al.,2022； Saleh et al., 2021), hence this paper used PLA as the rigid surface material. The high-speed camera system mainly included one high-speed digital camera (DSC-RX100M4, Sony Digital Products Co., Ltd., China), two sliding guide rails, two linear slide block bearings (SCS8), four shaft support seats (SK8), a fixing plate (PLA), and one spherical universal mount. The camera

can move within the range of + 110 mm to + 430 mm along the x-axis on the guide rails, ensuring that the digital camera's high-frame rate captured the tested fruit and the steel ruler's maximum range. Additionally, once the camera was positioned at a specified position, it could be adjusted to achieve the desired shooting angle in the right YOZ half-plane using the spherical universal mount, thereby meeting the experimental shooting requirements.

2.2.2 The development of the pad

Given the relatively small diameter of the impact rod, direct contact between the rod and the test fruit could result in a substantial rigid impact at the contact point of the fruit. In severe cases, it may even penetrate the fruit, hindering smooth ejection. Therefore, the design of the pad was of utmost importance. During the impact testing of the fruit, the internal impact force of the launching rod was transmitted to the test fruit through the pad, causing the rigid pad to pop up together with the fruit to be tested (Fig. 3). Impact testing was employed to examine the connection between dynamic force, specifically impact force, and time. It was important to note that the duration of the impact process was extremely short, typically lasting only a few milliseconds. During the launching of the fruit, the impact of the launching rod was the main source of kinetic energy provided to the fruit to achieve the initial velocity. The contact damage caused by this impact process was inevitable. However, it was worth noting that the impact force of the launching rod only affected the left end of the test fruit. Since the primary focus of this instrumented horizontal impactor was to investigate the relationship between impact force and time when the right end of the test fruit came into contact with the rigid plate, any mechanical damage caused by the launching rod to the test fruit did not influence the results of this experiment.

2.2.3 The development of the ejection port chuck

The chuck positioned at the ejection port served the crucial function of positioning and securing

158 the test fruit, a critical prerequisite for the successful execution of horizontal impact tests on fruit.
159 The precision with which the fruit was placed and the angle at which it was positioned directly
160 affected the accuracy of the test data. Therefore, the chuck design played a pivotal role in this study.
161 V-shaped chucks tailored for securing cherry tomatoes, plums, sweet cherries, and jujubes were
162 specifically developed to accommodate the variations in fruit types, sizes, and shapes. The V-shaped
163 opening stabilized the fruit's placement, thereby ensuring precise positioning during testing.
164 Additionally, the V-shaped design of the launching mouth served to minimise the frictional force
165 exerted on the test fruit during the ejection process. This reduction in friction reduced torque and
166 prevented the test fruit from undergoing substantial rotational motion after ejection. The chuck was
167 designed with upper and lower components. The upper part was connected to the launching tube of
168 the launcher through a circular interference fit, while the lower part was linked to the upper part using
169 adjustable bolts. Its primary function was to securely position the test fruit within the groove of the
170 lower part. By adjusting the connecting bolts between the upper and lower parts, the vertical position
171 of the fruit could be modified to shift the fruit's center of mass. This adjustment ensured that the center
172 of mass of fruit of varying sizes aligned with the central axis of the launching tube and the rigid
173 surface while maintaining a vertically oriented position relative to the rigid surface. Consequently,
174 this refinement enhanced the precision of the testing process.

175 ***2.3 Horizontal impact test***

176 ***2.3.1 Impact test measurement method***

177 In this study, we used "American Cherry No. 2" cherry tomatoes, "Red Heart Plum" plums,
178 "American Early" sweet cherries, and "Dali" winter jujubes as test materials. Fresh cherry tomatoes,
179 plums, sweet cherries, and winter jujube fruit were hand-harvested at the commercial ripening stage.
180 They were carefully inspected to ensure they were free from damage or insect infestations. The cherry

tomato, plum, sweet cherry and winter jujube fruit with similar size and shape were selected and immediately transported to the laboratory of Agri-Biomechanics research group, and the quantity of each type of fruit is 54 (3 buffer materials x 3 speed levels x 6 samples). Subsequently, they were manually cleaned with water, dried, and stood at room temperature (22 ± 1 °C, 50 ~ 55 % RH) for 24 h before being subjected to the impact test.

Prior to conducting the impact tests, each group of fruit was carefully arranged, and the initial mass of each fruit was individually recorded. Subsequently, the collisions were executed in a specific sequence, progressing from no cushioning to foam cushioning and expandable polyethylene (EPE) pearl cotton cushioning. Each cushioning material was subjected to collisions across three speed modes: slow, medium, and high. Changes in impact force overtime were recorded throughout the collisions, after each collision, and the entire motion process. After the completion of each collision, the test fruit were arranged according to the established testing order. Measurement indexes such as displacement, displacement rate, impact energy, and duration of impact process were recorded. This study used sweet cherry as the test material to evaluate the degree of impact damage and bruise susceptibility of fruit. Sweet cherry fruits were stored at room temperature after the impact tests, and the stored fruits were weighed daily to determine the mass loss rate (Romero and Lafuente., 2020). After 2 d of storage, the browning of sweet cherries in cross-section was assessed, and the extent of browning was quantified to evaluate the damage to sweet cherries under different cushioning materials and impact velocities.

2.3.2 Output parameters

2.3.2.1 Extraction of impact force and impact time

A planar membrane box-type pressure sensor (model: JHBM-H) was chosen to acquire data on impact force and impact time, including compression time and rebound time. Before testing, the

pressure sensor was connected to the data acquisition card, and ART measurement and control software was used to record the impact force and impact time data. Due to the short duration of the impact process and taking into account the test operation time and the time for the fruit to travel from the ejection port to the rigid plate, the data acquisition card was configured with a sampling rate of 20 KS/s and a duration of 10 seconds. This ensured that each test had ample operating time to collect complete impact force and impact time data.

2.3.2.2 Calculation of impact velocity, rebound velocity and absorption energy

The launcher had the capacity to propel 7.5 g steel balls at three different velocity levels: slow, medium, and high, corresponding to 5.4 m/s, 6.6 m/s, and 7.7 m/s, respectively. Based on the principle of energy conservation, we established:

$$\frac{1}{2}m_{\mathrm{b}}{v_{\mathrm{b}}}^{2}=\frac{1}{2}(m_{\mathrm{f}}+m_{r}){v_{\mathrm{f}}}^{2}+\mu_{\mathrm{f}}(m_{\mathrm{f}}+m_{\mathrm{r}})\mathrm{g}S_{\mathrm{f}}+E_{\mathrm{L}} \quad (1)$$

The mass range of the test fruit was determined through experiments, with the mass of the rigid pad m_{r} approximately 0.004 kg, a friction coefficient μ_{f} of 0.5, a sliding distance S_{f} of approximately 20 mm, and the energy loss E_{f} of fruit in inelastic collision was taken as 31.8 % (Celik., 2017). The theoretical horizontal launch velocities v_f for the test fruit in the slow-speed, medium-speed, and high-speed modes was calculated using Equation (1).

The high-speed camera system was capable of capturing the real-time motion of the test fruit, as shown in Fig. 3. To obtain the actual average initial velocity v_0 of the test fruit when it horizontally collided with the rigid surface and the rebound velocity v_1 of the test fruit, the Adobe After Effects software (Version: 2020, Adobe Systems Incorporated, USA) was used to process the motion videos of the experimental fruit captured by the high-speed camera. The video frame at the ejection mouth was recorded as the starting frame. Δt_0 represents the time it took for the test fruit to move 10 frames after the starting frame. During this time, the horizontal displacement of the test fruit's motion was

recorded as x_0. The average horizontal velocity of the test fruit after ejection was calculated using Equation (2). Considering the relatively short distance the fruit moved from the ejection mouth to the rigid plate, and ignoring air resistance, this calculated velocity could be regarded as the average initial velocity of the horizontal collision between the experimental fruit and the rigid surface. Similarly, the video frame at which the test fruit left the rigid plate was recorded as the rebound frame. Δt_1 represented the time it took for the test fruit to move 5 frames after the rebound frame. During this time, the horizontal displacement of the test fruit's motion was recorded as x_1. The rebound velocity v_1 of the test fruit was calculated using Equation (3). Using Equation (4), the relative error between the actual horizontal launch velocity and the theoretical horizontal launch velocity was calculated. Relative errors within the range of 5 % to 10 % were typically considered to indicate a small difference between the actual and theoretical values. The absorption energy E_0 of the test fruit was calculated using Equation (5) (Xu et al.,2019).

$$v_0 = \frac{x_0}{\Delta t_0} \tag{2}$$

$$v_1 = \frac{x_1}{\Delta t_1} \tag{3}$$

$$\epsilon = \frac{|v_0 - v_\mathrm{f}|}{v_\mathrm{f}} \times 100\ \% \tag{4}$$

$$E_0 = E_1 - E_2 = \frac{1}{2} m_\mathrm{f} v_0^2 - \frac{1}{2} m_\mathrm{f} v_1^2 \tag{5}$$

2.3.2.3 Calculation of damage parameters

Often, the damaged areas of test fruit were difficult to distinguish within a short period. For instance, in the case of sweet cherries, ripe ones exhibit a darker color, and since sweet cherry fruit were relatively small, discerning the color of the browned area from the unbrowned area was challenging with the naked eye. Due to the crushing of the part of the sweet cherry fruit involved in the collision process, damage occurred to the internal cells. Over time, the color of the affected cell area changed, and this outcome could be observed under a microscope. In this paper, the ratio of the

area of the browning region in the collision part of the longitudinal section of the fruit stalk axis to the total area of the longitudinal section of the stalk axis was used to estimate the degree of damage to the test fruit. The area of the browning region to the total area was quantified using Digimizer Version 5.4.4 through image analysis. The percentage of damaged area A_{d} was calculated by Equation (6). The fruit bruise susceptibility B_{d} was calculated by the ratio of the browning region area S_d to the absorption energy E_0 in Equation (7), which represents the ability of the fruit to withstand external impact (Yao et al., 2017). Additionally, the degradation in the quality of the test fruit following collision became evident after a period of storage, possibly associated with internal damage to the fruit. The rate of quality loss of the fruit on the first day A_{m1} was calculated using Equation (8), and the rate of quality loss of the fruit on the second day A_{m2} was calculated using Equation (9).

$$A_d = \frac{S_{\mathrm{d}}}{S_0} \times 100\,\% \tag{6}$$

$$B_{\mathrm{d}} = \frac{S_d}{E_0} \tag{7}$$

$$A_{\mathrm{m1}} = \frac{m_{\mathrm{d1}}}{m_{\mathrm{f}}} \times 100\,\% \tag{8}$$

$$A_{\mathrm{m2}} = \frac{m_{\mathrm{d2}}}{m_{\mathrm{f}}} \times 100\,\% \tag{9}$$

2.4 Statistical analysis

Multivariate analysis of variance (MANOVA) were performed using SAS software, version 9.2 (SAS Institute Inc., Cary, NC). The Fisher's least significant difference method was used for multiple comparison tests in MANOVA. The significance level was set at 0.05. Data were expressed as means ± standard deviation (SD).

3 Results and discussion

3.1 The performance of the new instrumented impactor

The properties of the self-developed instrumented horizontal impactor are presented in Table 1. The movement of the rigid plate along the X-axis direction was 25 mm, with an adjustment range spanning from - 12.5 mm ~ + 12.5 mm and an adjustment accuracy of 0.02 mm. The distance between the rigid plate and the ejection port measured 80 mm at its minimum position. Consequently, the adjustable range for the distance between the rigid plate and the ejection port along the X-axis direction extended from + 80 mm ~ + 105 mm. The distance between the high-speed camera and the ejection port along the Z-axis direction was 250 mm, and the adjustment range of the high-speed camera along the X-axis direction of the guide rail was + 110 mm ~ + 430 mm. This range ensured that the new type of the instrumented horizontal impactor could capture the screen range of + 190 mm ~ + 370 mm along the X-axis direction. The switching-mode power supply provided the entire device with a 12 V operating voltage. The force data sampling operated at an efficiency of 20 kS/s, while the image acquisition rate was 1000 frames per second (FPS). The impactor could provide speed levels as indicated in Table 2, including a slow-speed ejection range of 2.52 m/s ~ 3.17 m/s, a medium-speed ejection range of 2.97 m/s ~ 3.86 m/s, and a high-speed ejection range of 3.28 m/s ~ 4.38 m/s. The actual ejection speed was influenced by various factors, such as the fruit varieties and the quality of the fruit. There existed a slight difference between the theoretical ejection velocity and the actual ejection velocity, with an average relative error of less than 10 %. This disparity was primarily attributed to friction and other energy losses. The high-speed camera system captured the entire impact motion state of the fruit, as depicted in Fig. 4. This included the following stages: the initial position of the fruit, the launching process, the start in compression phase, the compression process; the maximum deformation position, the maximum deformation position, the recovery phase process, the rebound process, the rebound and descent process and the final status. In comparison with the pendulum-type device developed by Van Zeebroeck et al.（2007）, the entire inelastic impact

process of the fruit could be distinctly observed, and damage area could be distinguished using the self-developed instrumented horizontal impactor. This instrumented horizontal impactor enhanced the convenience of simulating horizontal impact damage and predicting damage areas in fruit.

3.2 Mechanical parameters for different collision conditions

Table 3 showed the impact mechanical parameters of different fruit under different collision conditions in high-speed mode, as measured using the self-developed instrumented horizontal impactor. The mean values of the mechanical parameters for various cushioning materials of different fruit were employed to assess the impact strength and degree of damage to the fruit. The results revealed that, when assessing various impact buffer materials for the same type of fruit, the average maximum impact force followed this descending order: rigid surface > foam board > EPE board. The average impact time followed this descending order: EPE board > foam board > rigid surface. Similarly, the average compression time ranked in descending order as EPE board > foam board > rigid surface. Whereas, the average energy absorption was highest for EPE board, followed by foam board and rigid surface. In comparison to the rigid plate surface, under the EPE pearl cotton impact conditions, the average maximum impact force for the four fruits decreased by more than 20 %, while the average impact time increased by more than 30 %, and the average energy absorption increased by over 30 %. The EPE board effectively mitigated the maximum impact force during the fruit impact process, extending both the impact time and compression time, and increasing energy absorption. This findings align with the impact characteristics and mechanical damage protection properties of EPE materials observed in studies on pears (Zhou et al., 2008), apples (Jarimopas et al., 2006), and peaches (Lin et al., 2020).

The results of variance analysis revealed significant differences in the maximum impact force, impact time, and compression time of the four fruits between the EPE board collision type and the rigid surface collision type. This could be attributed to the high ductility of EPE pearl cotton (Sunthar et al., 2020), enabling it to deform upon impact without immediate rupture. This property facilitated the dispersion of impact over time, thereby prolonging the impact process and reducing the peak value of the maximum impact force. Furthermore, the rebound velocity, rebound energy, and energy absorption of the four fruits under the EPE board collision type significantly differed from those under the rigid surface collision type. This could be attributed to the unique structure and material properties of EPE pearl cotton, consisting of numerous tiny bubbles capable of compression and deformation upon impact (Hassani et al., 2013; Manafi et al., 2019). This deformation could absorb the impact energy, converting it into heat and deformation energy, thereby diminishing the transmission and impact force. Consequently, by absorbing and dispersing impact energy, appropriate packaging materials could reduce impact force to the level that did not cause damage to the fruit. This capability minimizes fruit damage during transportation, storage, and handling.

Specifically, under the same cushioning material, the average maximum impact force of different fruit followed the following order: winter jujube > sweet cherry > plum > cherry tomato. The average impact time followed the order: cherry tomato > plum > sweet cherry > winter jujube. Lastly, the average energy absorption followed the order: cherry tomato > plum > sweet cherry > winter jujube. The degree of impact experienced by different fruit under the same velocity mode was associated with their biomechanical properties, including texture and density, elasticity, outer skin and shell layers, internal structure, and water content (Hou et al., 2016; An et al., 2020). Cherry tomatoes exhibited the smallest average maximum impact force, the longest average impact duration, and the highest average energy absorption compared to other fruit. This could be attributed to the

relatively thinner skin, softer internal flesh, and better elasticity and deformability of cherry tomatoes (Sun et al., 2021). These characteristics enabled cherry tomatoes to deform more readily when subjected to impacts, allowing them to absorb and disperse impact energy more effectively. As a result, this mitigated the propagation and concentration of impact forces. Conversely, the structure of winter jujube fruit is dense, and the relatively hard core of the fruit increases its overall hardness during impact (Huang et al., 2016). The presence of the fruit core further contributed to the reduced likelihood of deformation and dispersion of impact energy in winter jujube fruit when subjected to impact. This ultimately results in the largest average maximum impact force, the shortest average impact time, and the smallest average energy absorption.

3.3 Damage assessment for different crash conditions

3.3.1 The effect of different collision conditions on maximum impact force.

To assess the extent of horizontal impact damage to sweet cherries under various collision conditions, Fig. 5A illustrates a typical curve depicting the change in impact force recorded by the pressure sensor overtime during the horizontal impact test of sweet cherry fruit. Notably, the impact force during the horizontal impact on sweet cherry fruit initially rose and subsequently decreased with time. The collision process of fruit could be divided into two distinct stages: the compression and recovery stages. The stage during which the impact force increased over time was referred to as the compression stage, while the stage where the impact force decreases over time was known as the recovery stage (Li et al., 2017; Du et al., 2019). The complete collision process of the sweet cherry fruit, as depicted in this curve, spanned approximately 5 ms, with the compression phase lasting about 2 ms. In Fig. 5B, a comparative chart illustrated the maximum impact force generated under various collision types, with "speed 1", "speed 2" and "speed 3" representing slow speed, medium speed, and high speed, respectively. As depicted in the figure, when the initial speed was set at the slow speed

and the contact surfaces were EPE board, foam board, and rigid surface, the average maximum impact forces during the collision of sweet cherry fruit were as follows: 25 N, 29 N, and 33 N, respectively. Similarly, when the initial speed was at the medium level, and the contact surfaces were EPE board, foam board, and rigid surface, the average maximum impact forces during the collision of sweet cherry fruit were 32 N, 38 N, and 44 N, respectively. Furthermore, when the initial speed was set to high speed and the contact surfaces were EPE board, foam board, and rigid surface, the average maximum impact forces during the collision of sweet cherry fruit were: 35 N, 46 N, and 48 N, respectively. The results indicated that when sweet cherries collided with the foam board surface at three different speed modes (slow speed, medium speed, and high speed), the average maximum impact force was reduced compared to that on the rigid plate surface. Specifically, the reduction percentages were 8 % at slow speed, 17 % at medium speed, and 8 % at high speed. When sweet cherries collided with the EPE board surface at three different speed modes (slow speed, medium speed, and high speed), the average maximum impact force was reduced by 28 %, 36 %, and 32 %, respectively. This observation suggested that the buffer material effectively diminishes the impact force experienced by the fruit during the collision process (Zhou et al., 2016). Furthermore, it was evident that different cushioning materials exhibited varying abilities to reduce impact force (Avalle et al., 2001). Compared with foam board, EPE board performed better during the sweet cherry collision buffering effect.

3.3.2 The effect of different collision conditions on mass loss rate.

Sweet cherries could undergo quality degradation after a period of storage following collisions, which might be linked to internal damage. As a result, this study conducted separate assessments of the mass loss of sweet cherries after being stored for 1 d and 2 d following impacts against three different material surfaces at three distinct initial velocities. The results are depicted in Fig. 5C and

5D. According to the figures, the initial velocity and contact surface material impacted the mass loss rate of sweet cherries after collisions. Fig. 5C illustrated the mass loss of sweet cherries after 1 d storage following collisions. When the initial speed was set to slow speed, and the contact surfaces included EPE board, foam board, and rigid surface, the average mass loss rates were 5 %, 5 %, and 5 %, respectively. Similarly, when the initial speed was adjusted to medium speed, and the contact surfaces consisted of EPE board, foam board, and rigid surface, the average mass loss rates were 5 %, 6 %, and 6 %, respectively. Furthermore, when the initial speed was set to high speed, and the contact surfaces were EPE board, foam board, and rigid surface, the average mass loss rates were 5 %, 6 %, and 7 %, respectively. Fig. 5D showed the mass loss of sweet cherries after 2 d storage following collisions. When the initial speed was set to slow speed, and the contact surfaces included EPE board, foam board, and rigid surface, the average mass loss rates were 11 %, 12 %, and 13 %, respectively. Similarly, when the initial speed was adjusted to medium speed, and the contact surfaces consisted of EPE board, foam board, and rigid surface, the average mass loss rates were 12 %, 13 %, and 13 %, respectively. In addition, when the initial speed was set to high speed, and the contact surfaces were EPE board, foam board, and rigid surface, the average mass loss rates were 13 %, 14 %, and 17 %, respectively. The results indicated that the higher the initial velocity, the greater the mass loss rate of sweet cherries. This observation might be attributed to the formation of micro-cracks on the surface of sweet cherries following the collision. During the storage period, water tended to seep out from the areas of sweet cherries that were involved in the collision. The cells that became damaged due to the impact lost their ability to exchange materials and could not prevent water loss within the cells, leading to water seepage from within the fruit. With a higher initial speed, the fruit experienced a more significant impact force during the collision, resulting in more severe damage.

3.3.3 The influence of different collision conditions on the degree of damage

In Fig. 5G, a microscopic comparison between the area with and without collision damage is depicted. Meanwhile, Fig. 5E presents statistical data on the damage area observed in the longitudinal section of sweet cherries after 2 d of storage following collisions. The figure illustrated that when the initial speed was set to slow speed, and the contact surfaces included EPE board, foam board, and rigid surface, the average damage areas of the sweet cherry longitudinal section were 14 mm^2, 31 mm^2, and 40 mm^2, respectively. Similarly, when the initial speed was adjusted to medium speed, and the contact surfaces consisted of EPE board, foam board, and rigid surface, the average damage areas of the sweet cherry longitudinal section were 30 mm^2, 47 mm^2, and 69 mm^2, respectively. Additionally, when the initial speed was set to high speed, and the contact surfaces were EPE board, foam board, and rigid surface, the average damage areas of the sweet cherry longitudinal section were 58 mm^2, 103 mm^2, and 130 mm^2, respectively. Fig.5F shows the ratio of the damage area of the longitudinal section to the total area of the longitudinal section when sweet cherries were stored for 2 d after collision. When the initial speed was set to slow speed, and the contact surfaces include EPE board, foam board, and rigid surface, the average ratios of the damage area in the longitudinal section of sweet cherries to the total longitudinal section area were 2 %, 5 %, and 7 %, respectively. Also, when the initial speed was set to medium speed, and the contact surfaces consisted of EPE board, foam board, and rigid surface, the average ratios of the damage area of the longitudinal section of sweet cherries to the total area of the longitudinal section were 5 %, 9 %, and 12 % respectively. Furthermore, when the initial speed was at high speed, and the contact surfaces were EPE board, foam board, and rigid surface, the average ratios of the damage area in the longitudinal section of sweet cherries to the total longitudinal section area were 11 %, 18 %, and 23 %, respectively. The results indicated that the initial speed and the contact surface material impact the damage sustained by sweet cherries following collisions. Notably, higher initial speeds result in larger damage areas in sweet cherries. From a

mechanical perspective, when a fruit experienced an impact force, the individual cells within the fruit undergo distortion and deformation, leading to the stretching of the cell walls and, ultimately, rupture (Ferreira et al., 2008; Paulsen et al., 2019). Cell rupture generates significant reactive oxygen species (ROS), resulting in a notable increase in cell membrane lipid peroxidation levels. This increase led to heightened activities of phospholipase D (PLD), lipase, and lipoxygenase (LOX), ultimately compromising the integrity of the cell membrane (Lin et al., 2017; Mditshwa et al., 2018). Consequently, cells lost their ability to regulate internal components and intracellular water was lost. At a macroscopic level, the fruit became softened, and this type of damage was called bruising (Polat et al., 2012). Therefore, the horizontal impact test bench was used to simulate the horizontal impact between fruit and the surface of commercial packaging lines while capturing the motion and stress experienced by fruit during horizontal impacts. This approach, combined with experimental data, allowed for the exploration of the effects of various horizontal impact conditions on fruit damage. This was of great significance for predicting the rate and extent of fruit damage, reducing fruit quality degradation, enhancing the competitiveness of fruit in domestic and international markets, and increasing the income of fruit farmers.

4 Conclusion

This study developed a novel high-precision instrumented horizontal impactor to address the horizontal collision behavior between fruit and rigid plates in actual transportation processes. Horizontal impact tests were conducted, employing cherry tomatoes, plums, sweet cherries, and winter jujubes as experimental subjects, with impact initial velocity and cushioning material type as the experimental factors. The results confirmed that the developed novel high-precision instrumented horizontal impactor could effectively simulate the horizontal collision process between fruit and packaging materials. It provides output parameters including the impact force and the impact time of

fruit acting on each packaging material, as well as the displacement, displacement rate, impact energy, rebound energy, and absorption energy of the fruit. During horizontal collision simulation, the winter jujube exhibited the highest impact force and the shortest impact time compared to the other three types of fruit. When colliding with the EPE board, the sweet cherry exhibited the lowest proportion of damage area compared to collisions with the rigid board and foam board. The results of variance analysis indicated significant differences in the maximum impact force, impact time, and compression time of the four fruits between the EPE board collision type and the rigid surface collision type. The horizontal impactor introduced in this paper can be utilized in future to studies to investigate horizontal collision damage mechanism and the damage prevention mechanism of packaging materials during the transportation of other vulnerable fresh fruits, such as strawberry, bayberry, and blueberry. Building upon this research, future studies can delve deeper into investigating the influence of rigid plate positioning and various packaging materials on fruit damage. This would provide valuable theoretical insights for the design of packaging solutions for delicate fresh fruits. Ultimately, this study presents a robust and powerful tool for assessing the horizontal collision behavior between fruit and packaging materials.

Credit authorship contribution statement

Minggang Wang: Conceptualization, Investigation, Resources, Data curation, Software, Validation, Writing-original draft. Mingwei Shi: Writing-review & editing. Zhiguo Li: Writing-review & editing, Supervision, Funding acquisition, Project administration. Tobi Fadiji: Writing-review & editing, Supervision. Guoxiong Song: Writing-review & editing, Supervision.

Declaration of Competing Interest

The authors declare that they have no known competing financial interests or personal relationships that could have appeared to influence the work reported in this paper.

Data availability

The data that has been used is confidential.

Acknowledgments

This work was supported by an International Cooperation Key Plan of Shaanxi Province (2022KWZ-12) and a High-End Foreign Expert Recruitment Program (G2022172006L).

References

An, X., Li, Z., Zude-Sasse, M., Tchuenbou-Magaia, F., Yang, Y., 2020. Characterization of textural failure mechanics of strawberry fruit. J. Food Eng. 282, 110016. https://doi.org/10.1016/j.jfoodeng.2020.110016.

Avalle, M., Belingardi, G., Montanini, R., 2001. Characterization of polymeric structural foams under compressive impact loading by means of energy-absorption diagram. Int. J. Impact Eng. 25 (5), 455-472. https://doi.org/10.1016/S0734-743X(00)00060-9.

Ahmadi, E., Ghassemzadeh, H., Sadeghi, M., Moghaddam, M., Zarif, S., Mier, M., 2012. Dynamic modeling of peach fruit during normal impact. J Food Process Eng. 35 (3), 483-504. https://doi.org/10.1111/j.1745-4530.2010.00603.x.

Celik, H., 2017. Determination of bruise susceptibility of pears (*Ankara variety*) to impact load by means of FEM-based explicit dynamics simulation. Postharvest Biol. Tec. 128, 83-97. https://doi.org/10.1016/j.postharvbio.2017.01.015.

Cevher, E., Oztekin Y., 2022. Prediction of bruise in peach with impact energy. J Food Process Eng. 45(3), e13969. https://doi.org/10.1111/jfpe.13969.

Chen, K., Xu, G., Tian, R., Jiang, J., Wu, K., Kuang, Y., Jiang, F., 2023. Development of konjac glucomannan based syringa essential oil film and its fragmented form for quality maintenance of citrus fruits. Food Packaging Shelf. 40, 101185. https://doi.org/10.1016/j.fpsl.2023.101185.

Dintwa, E., Van Zeebroeck, M., Ramon, H., Tijskens, E., 2008. Finite element analysis of the dynamic collision of apple fruit. Postharvest Biol. Tec. 49 (2), 260-276. https://doi.org/10.1016/j.postharvbio.2008.01.012.

Du, D., Wang, B., Wang, J., Yao, F., Hong, X., 2019. Prediction of bruise susceptibility of harvested kiwifruit (*Actinidia chinensis*) using finite element method. Postharvest Biol. Tec. 152, 36-44.

504 https://doi.org/10.1016/j.postharvbio.2019.02.013.
505 Ferreira, M., Sargent, S., Brecht, J., Chandler, C., 2008. Strawberry fruit resistance to simulated
506 handling. Sci. Agr. 65 (5), 490-495. https://doi.org/10.1590/S0103 - 90162008000500007.
507 Fu, H., Karkee, M., He, L., Duan, J., Li, J., Zhang, Q., 2020. Bruise patterns of fresh market apples
508 caused by fruit-to-fruit impact. Agronomy, 10(1), 59.
509 https://doi.org/10.3390/agronomy10010059.
510 Hou J., Sun Y., Chen F., Liu C., 2016. Analysis of microstructures and macrotextures for different
511 apple cultivars based on parenchyma morphology. Microsc. Res. Techniq. 79 (4), 304-312.
512 https://doi.org/10.1002/jemt.22631.
513 Hussein, Z., Fawole, O., Opara, U., 2019. Bruise damage susceptibility of pomegranates (*Punica*
514 *granatum, L.*) and impact on fruit physiological response during short term storage. Hortic. 246
515 (27), 664-674. https://doi.org/10.1016/j.scienta.2018.11.026.
516 Hassani, M., Zarghami, R., Norouzi, R., Mostoufi N., 2013. Numerical investigation of effect of
517 electrostatic forces on the hydrodynamics of gas–solid fluidized beds. Powder Technol. 246, 16-
518 25. https://doi.org/10.1016/j.powtec.2013.05.007.
519 Huang, J., Zhang, C., Zhao, X., Fei, Z., Wan, K., Zhang, Z., Pang, X., Yin, X., Bai, Y., Sun, X., Gao,
520 L., Li, R., Zhang, J., Li, X., 2016. The jujube genome provides insights into genome evolution
521 and the domestication of sweetness/acidity taste in fruit trees. Plos. Genet. 12 (12), e1006433.
522 https://doi.org/10.1371/journal.pgen.1006433
523 Jarimopas, B., Singh, S., Sayasoonthorn, S., Singh J.,2006. Comparison of package cushioning
524 materials to protect post-harvest impact damage to apples. Packag Technol. 20(5), 315-324.
525 https://doi.org/10.1002/pts.760.
526 Li, Z., Andrews, J., Wang, Y., 2017. Mathematical modelling of mechanical damage to tomato fruit.

527 Postharvest Biol. Tec. 126, 50-56. https://doi.org/10.1016/j.postharvbio.2016.12.001.
528 Li, Z., Thomas, C., 2014. Quantitative evaluation of mechanical damage to fresh fruit. Trends Food
529 Sci. Tech. 35 (2), 138-150. https://doi.org/10.1016/j.tifs.2013.12.001.
530 Lin, Y., Lin, H., Shi, J., Chen, Y., Wang, H., 2017. Inhibitory effects of propyl gallate on membrane
531 lipids metabolism and its relation to increasing storability of harvested longan fruit. Food Chem.
532 217, 133-138. https://doi.org/10.1016/j.foodchem.2016.08.065.
533 Lin, M., Chen, J., Chen, F., Zhu, C., Wu, D., Wang, J., Chen, K., 2020. Effects of cushioning materials
534 and temperature on quality damage of ripe peaches according to the vibration test. Food
535 Packaging Shelf. 25, 100518. https://doi.org/10.1016/j.fpsl.2020.100518.
536 Manafi, M., Zarghami, R., Mostoufi, N., 2019. Effect of electrostatic charge of particles on
537 hydrodynamics of gas-solid fluidized beds. Adv Powder Technol. 30 (4):815-828.
538 https://doi.org/10.1016/j.apt.2019.01.010.
539 Mditshwa, A., Fawole, O., Opara, U., 2018. Recent developments on dynamic controlled atmosphere
540 storage of apples-A review. Food Packaging Shelf. 16, 59-68.
541 https://doi.org/10.1016/j.fpsl.2018.01.011.
542 Ortiz, C., Torregrosa, A., 2014. Mechanical properties of citrus and impact damage under different
543 storage conditions. T. Asabe. 57 (2), 593-598. https://doi.org/10.13031/trans.57.10479.
544 Öztekin, Y., Güngör, B., 2020. Determining impact bruising thresholds of peaches using electronic
545 fruit. Sci. Hortic. 262, 1-6. https://doi.org/10.1016/j.scienta.2019.109046.
546 Polat, R., Aktas, T., Ikinci, A., 2012. Selected mechanical properties and bruise susceptibility of
547 nectarine fruit. Int. J. Food Prop. 15, 1369-1380. https://doi.org/10.1080/10942912.2010.498546.
548 Polat, R., Gezer, I., Guner, M., Dursun, E., Erdogan, D., Bilim, H., 2007. Mechanical harvesting of
549 pistachio nuts. J. Food Eng. 79 (4), 1131-1135. https://doi.org/10.1016/j.jfoodeng.2006.03.023.

Preuk, C., Utto, W., Boonyaritthongchai, P., Wasusri, T., Wongs-Aree, C., 2019. Ethanol vapor releasing sachet reduces decay and improves aroma attributes in mulberry fruit. Food Packaging Shelf. 22,100398. https://doi.org/10.1016/j.fpsl.2019.100398.

Paulsen, E., Barrios, S., Lema, P., 2021. Production of packaged ready - to - eat whole strawberries (cv. *San Andreas*): Packaging conditions for shelf-life extension. Food Packaging Shelf. 29, 100696. https://doi.org/10.1016/j.fpsl.2021.100696.

Paulsen, E., Barrios, S., Lema, P., 2019. Ready-to-eat cherry tomatoes: Passive modified atmosphere packaging conditions for shelf life extension. Food Packaging Shelf. 22, 100407. https://doi.org/10.1016/j.fpsl.2019.100407.

Romero, P., Lafuente, M., 2020. Abscisic acid deficiency alters epicuticular wax metabolism and morphology that leads to increased cuticle permeability during sweet orange (*citrus sinensis*) fruit ripening. Front. Plant Sci. 11, 594184-594184. https://doi.org/10.3389/fpls.2020.594184.

Stropek, Z. and Golacki, K., 2019. Impact characteristics of pears. Postharvest Biol. Technol. 147, 100-106. https://doi.org/10.1016/j.postharvbio.2018.09.015.

Sunthar, T., Marin, E., Boschetto, F., Zanocco, M., Sunahara, H., Ramful, R., Kamei, K., Zhu, W., Pezzotti, G., 2020. Antibacterial and antifungal properties of composite polyethylene materials reinforced with neem and turmeric. antibiotics-basel. 9(12), 857. https://doi.org/10.3390/antibiotics9120857.

Sun, Y., Pessane, I., Pan, L., Wang, X., 2021. Hyperspectral characteristics of bruised tomatoes as affected by drop height and fruit size. LWT-Food Sci. Technol. 141, 110863. https://doi.org/10.1016/j.lwt.2021.110863.

Sun, K., Wang, Z., Zhang, X., Wei, Z., Zhang, X., Li, L., Fu, Y., Gao, J., Zhao, X., Guo, J., Wang, J., 2021. Enhancement of biocontrol efficacy of pichia kudriavzevii induced by ca ascorbate

against botrytis cinerea in cherry tomato fruit and the possible mechanisms of action. Microbiol. Spectr. 9 (3), e0150721. https://doi.org/10.1128/spectrum.01507-21

Shi, W., Chen, Z., 2022. Mechanical, rheological, and crystallinity properties of polylactic acid/polyethylene glycol-polydimethylsiloxane copolymer blends by melt blending. J Appl. Polym. 140(4), E53346. https://doi.org/10.1002/app.53346.

Saleh, M., Kempers, R., Melenka, G., 2021. A comparative study on the electromechanical properties of 3D-Printed rigid and flexible continuous wire polymer composites for structural health monitoring. Sensor Actuat A-Phys. 328, 112764. https://doi.org/10.1016/j.sna.2021.112764.

Tian, S., Fan, Q., Xu, Y., Wang, Y., Jiang, A., 2001. Evaluation of the use of high CO_2 concentrations and cold storage to control Monilinia fructicola on sweet cherries. Postharvest Biol. Technol. 22 (1), 53-60. https://doi.org/10.1016/S0925-5214(00)00177.

Van Zeebroeck, M., Tijskens, E., Van Liedekerke, P., Deli, J., De Baerdemaeker, J., Ramon, H., 2003. Determination of the dynamical behaviour of biological materials during impact using a pendulum device. J. Sound Vib. 266 (3), 465-480. https://doi.org/10.1016/S0022-460X(03)00579-0.

Van Zeebroeck, M., Lombaert, G., Dintwa, E., Ramon, H., Degrande, G., Tijskens, E., 2008. The simulation of the impact damage to fruit during the passage of a truck over a speed bump by means of the discrete element method. Biosyst. Eng. 101 (1), 58-68. https://doi.org/10.1016/j.biosystemseng.2008.06.003.

Van Zeebroeck, M., Van Linden, V., Darius, P., De Ketelaere, B., Ramon, H., Tijskens, E., 2007. The effect of fruit properties on the bruise susceptibility of tomatoes. Postharvest Biol. Technol. 45 (2), 168-175. https://doi.org/10.1016/j.postharvbio.2006.12.022.

Wang, W., Yang, Z., Lu, H., Fu, H., 2018. Mechanical damage caused by fruit-to-fruit impact of litchis.

IFAC-PapersOnline. 51 (17), 532-535. https://doi.org/10.1016/j.ifacol.2018.08.154.

Wang, W., Zhang, S., Fu, H., Lu, H., Yang, Z., 2020. Evaluation of litchi impact damage degree and damage susceptibility. Comput. Electron. Agric. 173, 105409. https://doi.org/10.1016/j.compag.2020.105409.

Xu, R., Takeda, F., Krewer, G., Li, C., 2015. Measure of mechanical impacts in commercial blueberry packing lines and potential damage to blueberry fruit. Postharvest Biol. Technol. 110, 103-113. https://doi.org/10.1016/j.postharvbio.2015.07.013.

Xu, D., Wang, H., Ji, H., Zhang, X., Cerbu, C., Hu, E., Dong F., 2019. Quantitative evaluation of impact damage to apple by hyperspectral imaging and mechanical parameters. Food Anal. Methods. 12, 371–380. https://doi.org/10.1007/s12161-018-1369-9.

Zhang, B., Zhou, J., Meng, Y., Zhang, N., Gu, B., Yan, Z., Idris, S. I., 2018. Comparative study of mechanical damage caused by a two-finger tomato gripper with different robotic grasping patterns for harvesting robots. Biosyst. Eng. 171, 245-257. https://doi.org/10.1016/j.biosystemseng.2018.05.003.

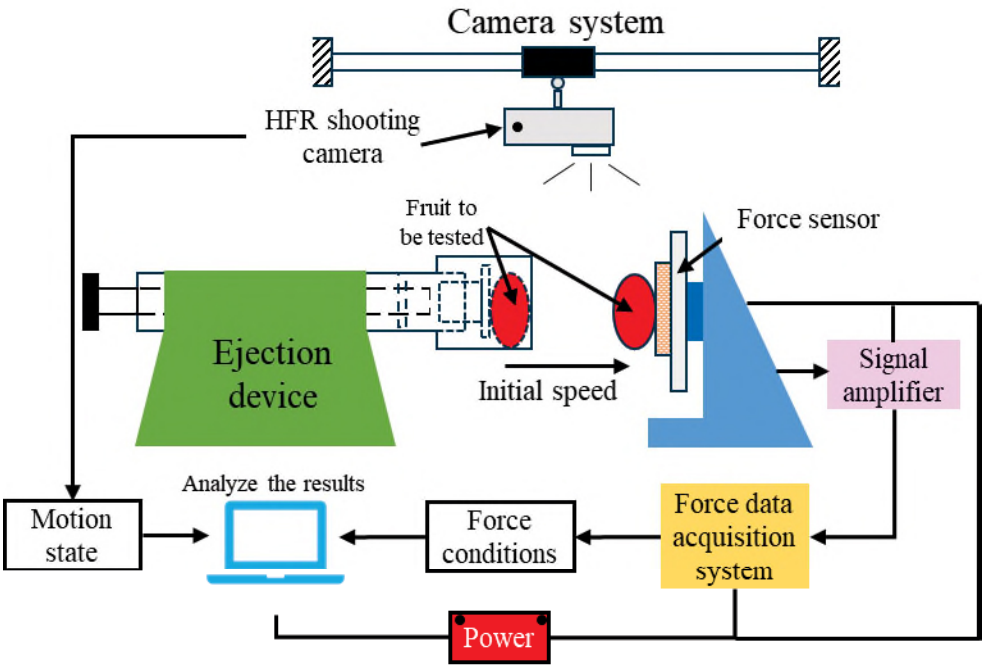
Zhou, J., He, L., Karkee, M., Zhang, Q., 2016. Effect of catching surface and tilt angle on bruise damage of sweet cherry due to mechanical impact. Comput. Electron. Agric. 121, 282-289. https://doi.org/10.1016/j.compag.2016.01.004.

Zhou, R., Su, S., Li, Y., 2008. Effects of cushioning materials on the firmness of Huanghua pears (*Pyrus pyrifolia Nakai cv. Huanghua*) during distribution and storage. Packag Technol. 21(1), 1-11. https://doi.org/10.1002/pts.769.

Zhou, J., He, L., Karkee, M., Zhang, Q., 2016. Analysis of shaking-induced cherry fruit motion and damage. Biosyst. Eng. 144, 105-114. https://doi.org/10.1016/j.biosystemseng.2016.02.007.

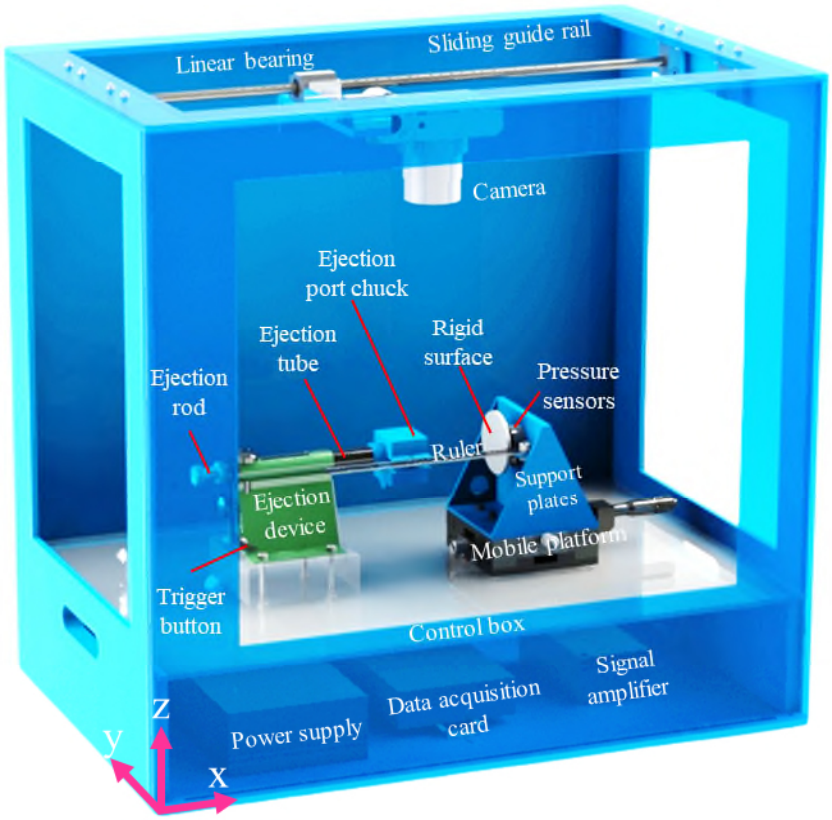
618 # Figures and Tables

619



620

621 **Fig. 1** The design concept of a new instrumented horizontal impactor.



622

623 **Fig. 2** The physical structure of the new instrumented horizontal impactor.

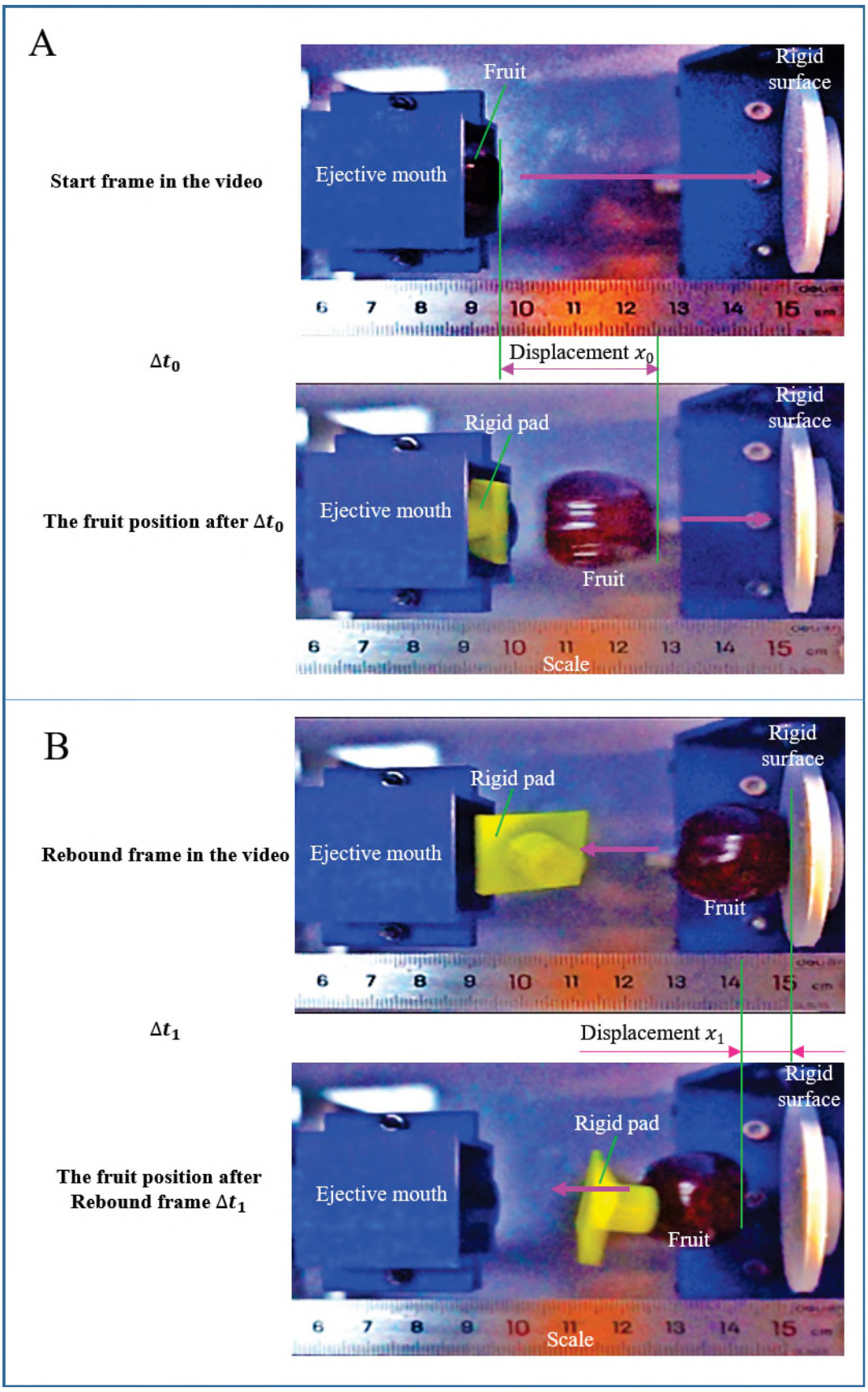


Fig. 3 The moving process of a fruit in the horizontal impact test video. (A) The process of fruit ejection movement; (B) The process of fruit rebound movement.

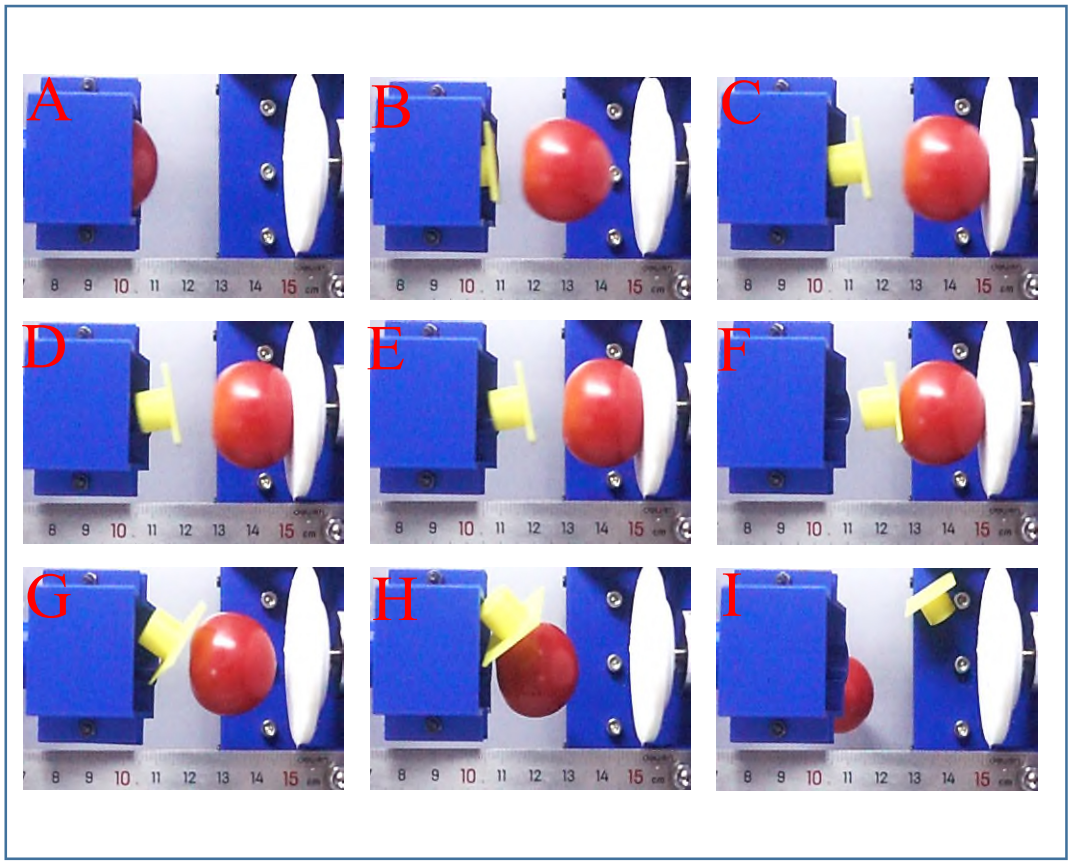


Fig. 4 The horizontal collision process between a sweet tomato and a rigid surface. (A) Initial position of the fruit; (B) The launching process; (C) The start in compression phase; (D) The compression process; (E) The maximum deformation position; (F) The recovery phase process; (G) The rebound process; (H) The rebound and descent process; (I) Final status.

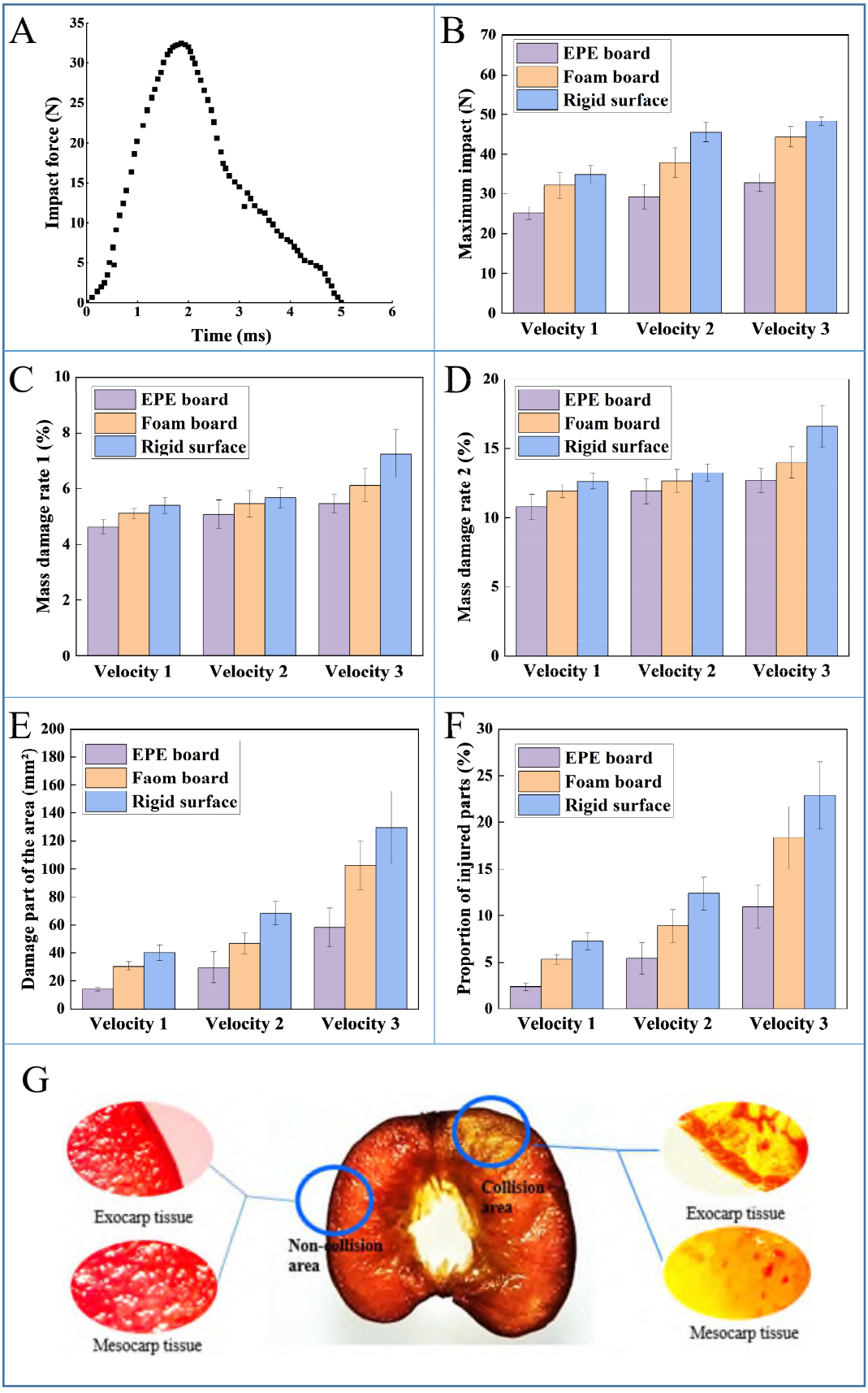


Fig. 5 The assessment of the degree of horizontal impact damage. (A) A typical impact force-time curve during horizontal collision process; (B) Effect of collision type and initial velocity on the

maximum impact force; (C) Mass loss rate of sweet cherry after 1 d storage in different collision type; (D) Mass loss rate of sweet cherry after 2 d storage in different collision type; (E) Damage area of sweet cherry during horizontal impact test; (F) Percentage of damage area of sweet cherry during horizontal impact test (G) Contrast of collision area with non-collision area.

639 **Table 1** The properties of the instrumented horizontal impactor

Properties	**Value**	**Properties**	**Value**
Mass	11.4 kg	Operating voltage	12 v
Length × Width× Height	520 × 340 × 500 mm	Force data sample rate	20 kS/s
Rigid plate X-axis movement	± 12.5 mm	Image acquisition rate	1000 FPS
Axial movement precision	0.02 mm	Force sensor sensitivity	2.0 ± 0.1 mv/v
Image capture range	+ 190 mm~+ 370 mm	Comprehensive accuracy	0.1 % F·S

640

641 **Table 2** Comparison between theoretical ejection velocity and actual ejection velocity

Fruit	Velocity Mode	m_f, g	V_f, m/s	V_0, m/s	ϵ
Cherry Tomato	Slow speed mode	16.31 ± 0.62	2.70 ± 0.09	2.79 ± 0.08	3.39 ± 1.84
	Medium speed mode	15.94 ± 1.24	3.32 ± 0.11	3.21 ± 0.24	3.14 ± 3.99
	High speed mode	15.83 ± 2.26	3.90 ± 0.23	3.81 ± 0.12	4.14 ± 2.33
Plum	Slow speed mode	15.99 ± 1.45	2.70 ± 1.45	2.64 ± 0.12	3.13 ± 2.97
	Medium speed mode	16.29 ± 1.01	3.29 ± 0.08	3.32 ± 0.05	1.76 ± 1.41
	High speed mode	15.77 ± 1.07	3.71 ± 0.30	3.55 ± 0.27	4.60 ± 3.73
Sweet Cherry	Slow speed mode	10.73 ± 1.27	3.16 ± 0.11	3.04 ± 0.13	3.90 ± 1.43
	Medium speed mode	10.76 ± 0.47	3.86 ± 0.06	3.77 ± 0.09	2.39 ± 1.72
	High speed mode	10.99 ± 0.64	4.48 ± 0.10	4.32 ± 0.06	3.71 ± 1.42
Winter jujube	Slow speed mode	14.19 ± 1.08	2.83 ± 0.09	2.66 ± 0.12	5.94 ± 2.74
	Medium speed mode	13.88 ± 0.89	3.51 ± 0.10	3.53 ± 0.02	1.92 ± 1.32
	High speed mode	13.17 ± 1.39	4.10 ± 0.12	3.82 ± 0.03	6.98 ± 2.18

642

643 **Table 3** The impact mechanical parameters of fruit under different collision type

Parameters	Collision type	Cherry Tomato	Plum	Sweet Cherry	Winter Jujube
V_0, m/s	Fruit-Rigid surface	3.81 ± 0.12^{a}	3.55 ± 0.27^{a}	4.32 ± 0.06^{b}	3.82 ± 0.03^{a}
	Fruit-Foam board	3.83 ± 0.14^{a}	3.72 ± 0.15^{a}	4.40 ± 0.06^{b}	3.87 ± 0.36^{a}
	Fruit-EPE board	3.91 ± 0.07^{a}	3.48 ± 0.19^{a}	4.74 ± 0.17^{a}	3.87 ± 0.08^{a}
V_1, m/s	Fruit-Rigid surface	1.49 ± 0.13^{a}	1.99 ± 0.11^{a}	2.83 ± 0.09^{a}	2.57 ± 0.27^{a}
	Fruit-Foam board	0.99 ± 0.18^{b}	1.66 ± 0.33^{b}	2.44 ± 0.12^{b}	2.04 ± 0.11^{b}
	Fruit-EPE board	0.50 ± 0.19^{c}	1.51 ± 0.06^{b}	2.56 ± 0.12^{b}	1.69 ± 0.38^{b}
F_{max}, N	Fruit-Rigid surface	44.98 ± 0.70^{a}	45.09 ± 2.34^{a}	48.28 ± 1.11^{a}	49.68 ± 0.46^{a}
	Fruit-Foam board	41.53 ± 1.37^{b}	41.54 ± 1.02^{b}	45.52 ± 2.44^{a}	45.94 ± 1.65^{b}
	Fruit-EPE board	30.47 ± 0.57^{c}	33.75 ± 0.99^{c}	34.86 ± 2.33^{b}	39.56 ± 1.02^{c}
t_I, ms	Fruit-Rigid surface	6.60 ± 0.21^{c}	5.48 ± 0.34^{c}	5.45 ± 0.16^{c}	2.93 ± 0.19^{c}
	Fruit-Foam board	7.64 ± 0.68^{b}	6.31 ± 0.12^{b}	5.88 ± 0.06^{b}	4.69 ± 0.46^{b}
	Fruit-EPE board	9.16 ± 0.84^{a}	8.02 ± 0.51^{a}	7.10 ± 0.08^{a}	5.94 ± 0.27^{a}
t_c, ms	Fruit-Rigid surface	2.90 ± 0.18^{b}	2.15 ± 0.09^{b}	2.13 ± 0.15^{b}	1.07 ± 0.05^{c}
	Fruit-Foam board	3.26 ± 0.19^{a}	2.59 ± 0.31^{a}	2.63 ± 0.29^{b}	1.58 ± 0.22^{b}
	Fruit-EPE board	3.56 ± 0.25^{a}	2.79 ± 0.29^{a}	3.02 ± 0.30^{a}	2.17 ± 0.22^{a}
E_1, 10^{-3}J	Fruit-Rigid surface	110.09 ± 15.01^{a}	94.66 ± 18.26^{a}	102.23 ± 4.09^{b}	95.80 ± 9.06^{a}
	Fruit-Foam board	116.33 ± 19.36^{a}	106.65 ± 5.66^{a}	101.55 ± 6.10^{b}	95.92 ± 9.31^{a}
	Fruit-EPE board	126.97 ± 8.12^{a}	101.06 ± 10.70^{a}	122.09 ± 8.04^{a}	105.32 ± 21.64^{a}
E_2, 10^{-3} J	Fruit-Rigid surface	16.96 ± 2.88^{a}	31.43 ± 3.81^{a}	44.17 ± 3.86^{a}	43.69 ± 10.25^{a}
	Fruit-Foam board	8.20 ± 3.68^{b}	21.92 ± 8.42^{b}	31.19 ± 1.67^{b}	26.50 ± 1.83^{b}
	Fruit-EPE board	2.33 ± 1.68^{c}	18.88 ± 1.86^{b}	35.70 ± 4.10^{b}	20.66 ± 9.17^{b}
E_0, 10^{-3} J	Fruit-Rigid surface	93.14 ± 13.59^{b}	63.23 ± 15.16^{b}	58.06 ± 3.50^{c}	52.11 ± 10.16^{b}
	Fruit-Foam board	108.13 ± 17.14^{ab}	84.73 ± 6.61^{a}	70.36 ± 6.79^{b}	69.42 ± 9.82^{ab}
	Fruit-EPE board	124.64 ± 7.77^{a}	90.18 ± 1.69^{a}	86.39 ± 5.29^{a}	84.67 ± 22.27^{a}
S_0, mm^2	Fruit-Rigid surface	\	\	129.66 ± 25.90^{a}	\
	Fruit-Foam board	\	\	102.54 ± 17.52^{b}	\
	Fruit-EPE board	\	\	58.16 ± 13.71^{c}	\
A_d	Fruit-Rigid surface	\	\	22.86 ± 3.61^{a}	\
	Fruit-Foam board	\	\	18.36 ± 3.33^{a}	\
	Fruit-EPE board	\	\	10.94 ± 2.33^{b}	\
B_d, 10^3 mm^2/J	Fruit-Rigid surface	\	\	2.40 ± 0.35^{a}	\
	Fruit-Foam board	\	\	1.49 ± 0.20^{b}	\
	Fruit-EPE board	\	\	0.68 ± 0.17^{c}	\
A_{m1}	Fruit-Rigid surface	\	\	7.28 ± 0.87^{a}	\
	Fruit-Foam board	\	\	6.12 ± 0.60^{b}	\
	Fruit-EPE board	\	\	5.44 ± 0.33^{b}	\
A_{m2}	Fruit-Rigid surface	\	\	16.59 ± 1.52^{a}	\
	Fruit-Foam board	\	\	13.98 ± 1.14^{b}	\
	Fruit-EPE board	\	\	12.68 ± 0.88^{b}	\

644
645 Note: Different superscript letters (namely, a, b, and c) in the same group indicate significant
646 differences according to ANOVA.



https://dspace.org/

Investigation of the horizontal collision damage behavior of fruit during transporting based on a new instrumented impactor

Wang, Minggang; Shi, Mingwei; Fadiji, Tobi; Li, Zhiguo; Song, Guoxiong

2024-07-01
Elsevier
https://doi.org/10.1016/j.postharvbio.2024.112977
Wang M, Shi M, Fadiji T, et al., (2024) Investigation of the horizontal collision damage behavior of fruit during transporting based on a new instrumented impactor. Postharvest Biology and Technology, Volume 213, July 2024, Article number 112977

Downloaded from a DSpace repository. https://dspace.org/